



Phylogenetic characters in the humerus and tarsometatarsus of penguins

Martín CHÁVEZ HOFFMEISTER

School of Earth Sciences, University of Bristol, Wills Memorial Building, Queens Road, BS8 1RJ, Bristol, United Kingdom and Laboratorio de Paleoecología, Instituto de Ciencias Ambientales y Evolutivas, Universidad Austral de Chile, Valdivia, Chile
<glmfch@bristol.ac.uk>

Abstract: The present review aims to improve the scope and coverage of the phylogenetic matrices currently in use, as well as explore some aspects of the relationships among Paleogene penguins, using two key skeletal elements, the humerus and tarsometatarsus. These bones are extremely important for phylogenetic analyses based on fossils because they are commonly found solid specimens, often selected as holo- and paratypes of fossil taxa. The resulting dataset includes 25 new characters, making a total of 75 characters, along with eight previously uncoded taxa for a total of 48. The incorporation and analysis of this corrected subset of morphological characters raise some interesting questions considering the relationships among Paleogene penguins, particularly regarding the possible existence of two separate clades including *Palaeudyptes* and *Parapterodytes*, the monophyly of *Platydyptes* and *Parapterodytes*, and the position of *Anthropornis*. Additionally, *Notodyptes wimani* is here recovered in the same collapsed node as *Archaeospheniscus* and not within *Delphinornis*, as in former analyses.

Key words: Sphenisciformes, limb bones, phylogenetic analysis, parsimony method, revised dataset.

Introduction

Since the work of O'Hara (1986), the phylogeny of penguins has been a subject of great interest. During the last decade, several authors have explored the use of molecular (*e.g.*, Subramanian *et al.* 2013), morphological (*e.g.*, Giannini and Bertelli 2004) and combined datasets (*e.g.*, Bertelli and Giannini 2005; Ksepka *et al.* 2006; Chávez Hoffmeister *et al.* 2014) in order to resolve the relationships among extant and extinct penguins. Despite persistent disagreement between morphological and molecular data regarding the rooting of the crown group (Ksepka and Ando 2011), there is a general consensus that the Paleogene (*i.e.*, early) penguins are arranged in a paraphyletic series leading to crown

Spheniscidae, the clade of modern penguins. This contrasts with the earlier taxonomic arrangements proposed by Simpson (1946) and Marples (1962), which suggested the existence of several distinctive clades of extinct penguins or “subfamilies”.

Currently, a vast majority of phylogenetic studies including fossil and extant taxa are based on the supermatrix of Ksepka *et al.* (2006) and its subsequent modifications (Clarke *et al.* 2007, 2010; Ksepka and Clarke 2010; Ksepka *et al.* 2012; Ksepka and Thomas 2013). The most recent version of this dataset included 254 morphological characters (Chávez Hoffmeister *et al.* 2014), of which 31 are from the humerus and 19 from the tarsometatarsus, representing 19.1% and 11.7% of the osteological characters respectively. These elements are extremely important for the incorporation of fossil penguin traits into phylogenetic matrices, being rather solid elements relatively abundant as fossils (Cruz 2005, 2007; Chávez Hoffmeister 2007) and informative enough to allow taxonomical identifications (see Walsh *et al.* 2007, 2008). As a result, both elements are widely used for the typification of fossil penguins and, in most cases, are the only elements that can be assigned with certainty to extinct taxa. The fossil penguins of the Eocene La Meseta Formation on Seymour Island, Antarctic Peninsula, are a clear example of this bias in the selection of type specimens: of the 15 described species, ten of the 11 based on tarsometatarsi are usually considered valid, whereas the four based on humeri and a synsacrum are often considered junior synonyms or *nomina dubia* (Myrcha *et al.* 2002; Ksepka and Clarke 2010; Jadwiszczak and Mörs 2011).

Despite recent efforts to assign isolated bones to taxa (erected on the basis of a modest fossil record) based on quantitative analyses (Jadwiszczak 2006; Jadwiszczak and Acosta Hospitaleche 2013), in most cases, only the discovery of associated specimens can offer conclusive evidence of their taxonomic identity. Nevertheless, the humerus and tarsometatarsus remain the best-known reference or “binding” skeletal elements. Unfortunately, some of these poorly known taxa tend to resolve in very different positions when included into phylogenetic analysis (wildcard taxa), reducing the performance of the analysis and the resolution of the consensus trees. A clear example of this is *Notodyptes wimani* Marples, 1953 from the La Meseta Formation, known only from incomplete and/or abraded tarsometatarsi (Marples 1953; Myrcha *et al.* 2002).

The purpose of this work is twofold: to improve the scope and coverage of the character matrices currently in use in studies of penguin phylogeny and to explore the relations among Sphenisciformes, in particular those from the Paleogene period. Here, I propose a revision of the characters in the humerus and tarsometatarsus, based on an extensive review of specimens. I also present a consensus tree resulting from the analysis of this dataset, discussing the scope and limitations of using these anatomical elements in studies of penguin evolution.

Material and methods

The following characters are based on the humerus/tarsometatarsus traits used by Chávez Hoffmeister *et al.* (2014), which in turn were modified from Ksepka *et al.* (2012) and Ksepka and Thomas (2013). Twenty-five new characters were added for a total of 75 humerus/tarsometatarsus traits. Examples of taxa showing each character state are given. Citation of figures is also offered for most characters. Characters that are new or have been significantly modified in respect to former studies are clearly indicated. The orientation use in the description of humerus characters is based on the homologous anatomical planes between penguins and non-penguin taxa, whereas the equivalent orientation for penguins in standing position is presented in parentheses. The corrected dataset can be consulted in Appendix 1, and a TNT file of the corrected subset can be downloaded from the profile of the author at ResearchGate.net.

The matrix has been assembled focusing on Paleogene penguins, including a total of 43 in-group taxa. As a result, most of the Paleogene taxa included in former analyses have been retained, with the exception of *Waimanu manningi* Slack, Jones, Ando *et Fordyce* (in Slack *et al.* 2006) and *Duntroonornis parvus* Marples, 1952. Both taxa were included during the preliminary analysis, but excluded from the final version in order to improve its performance. Eight taxa uncoded in former analyses were included here: *Crossvallia unienwillia* Tambussi, Reguero, Marensi *et Santillana*, 2005, *Kaiika maxwelli* Fordyce *et Thomas*, 2011, *Palaeodyptes marplei* Brodkorb, 1963, *Platydyptes amiesi* Marples, 1952, *Arthrodytes grandis* (Ameghino, 1901), *Paraptenodytes brodkorbi* Simpson, 1972, *Paraptenodytes robustus* (Ameghino, 1895) and the Hakataramea penguin (Fordyce and Jones 1990; Acosta Hospitaleche *et al.* 2004; Ando 2007). The crown and Neogene crown-ward taxa are represented by the fossil genera *Eretiscus* Olson, 1986, *Palaeospheniscus* Moreno *et Mecerat*, 1891 and *Madrynornis* Acosta Hospitaleche, Tambussi, Donato *et Cozzuol*, 2007 plus one species for each extant genus. The outgroup includes four species of Procellariiformes (*Diomedea exulans*, *Oceanodroma tethys*, *Pelecanoides urinatrix* and *Puffinus griseus*) and one species of Gaviiformes (*Gavia immer*). The trees were rooted to Gaviiformes.

The state of characters was verified and corrected for each taxon through direct observation of museum specimens (over 80% of the taxa) and by the use of bibliographical data and/or high-resolution photographs (Table 1). Multiple specimens were used when available in order to recognize polymorphic states. As a result, several states have been corrected in the matrix in order to offer a more accurate coding for each taxon.

In order to compare the resolution and performance of this corrected subset with results of former studies, I ran the analyses of three sets of humerus/ tarsometatarsus characters: (i) the uncorrected subset presented by Chávez Hoffmeister *et al.* (2014) (38 taxa, 50 characters); (ii) the corrected subset with an equivalent sample of taxa

Table 1

Sources of character coding for fossil penguin taxa

Taxon	Epoch	Specimens examined/References for coding
<i>Anthropornis grandis</i>	Eocene	Humeri: IB/P/B-0119, 0179. Tarsometatarsi: NHM A2002 (cast of holotype), A5574 (cast); IB/P/B-0483.
<i>Anthropornis nordenskjöldi</i>	Eocene	Humeri: NHM A338, A2013 (cast). Tarsometatarsi: NHM A2000 (cast of holotype); IB/P/B-0070.
<i>Archaeospheniscus lopdelli</i>	Late Oligocene	Tarsometatarsus: NHM A4080 (cast of holotype).
<i>Archaeospheniscus lowei</i>	Late Oligocene	Humerus: Simpson (1971), photographic record.
<i>Arthrodytes grandis</i>	Late Oligocene	Humerus: MLP 606 (cast of holotype).
Burnside “ <i>Paleeudyptes</i> ”	Late Eocene	Humerus: Photographical record.
<i>Crossvallia unienwillia</i>	Late Paleocene	Humerus: MLP 00-I-10-1 (holotype).
<i>Delphinornis arctowskii</i>	Late Eocene	Tarsometatarsi: IB/P/B-0484 (holotype); NHM A5578 (cast).
<i>Delphinornis gracilis</i>	Late Eocene	Tarsometatarsus: IB/P/B-0279a (holotype).
<i>Delphinornis larseni</i>	Eocene	Tarsometatarsi: NHM A2003 (cast of holotype), A5577 (cast); IB/P/B-0062.
<i>Eretiscus tonni</i>	Early Miocene	Humeri: MLP 62-III-29-25; MPEF-PV 507, 508. Tarsometatarsus: MLP 81-VI-26-1 (holotype).
<i>Hakataramea penguin</i>	Late Oligocene	Humerus: MLP 21977 (cast).
<i>Icadyptes salasi</i>	Late Eocene	Humerus: MUSM 897 (holotype).
<i>Inkayacu paracasensis</i>	Late Eocene	Humerus/Tarsometatarsus: MUSM 1444 (holotype).
<i>Kaiika maxwelli</i>	Early Eocene	Humerus: Fordyce and Thomas (2011), photographic record.
<i>Kairuku grebneffi</i>	Late Oligocene	Humerus/Tarsometatarsus: Ksepka <i>et al.</i> (2012).
<i>Kairuku waitaki</i>	Late Oligocene	Humerus/Tarsometatarsus: Ksepka <i>et al.</i> (2012).
<i>Madrynornis mirandus</i>	Middle Miocene	Humerus/Tarsometatarsus: MPEF-PV 100 (holotype).
<i>Marambiornis exilis</i>	Late Eocene	Tarsometatarsus: IB/P/B-0490 (holotype).
<i>Mesetaornis polaris</i>	Late Eocene	Tarsometatarsus: IB/P/B-0278 (holotype).
<i>Notodyptes wimani</i>	Eocene	Tarsometatarsi: NHM A3331 (holotype); IB/P/B-0491.
<i>Pachydyptes ponderosus</i>	Late Eocene	Humerus: NHM A3632 (cast of holotype).
<i>Palaeudyptes antarcticus</i>	Early Oligocene	Tarsometatarsus: NHM A1048 (holotype).
<i>Palaeudyptes gunnari</i>	Eocene	Humeri: IB/P/B-0306, 0472; MLP 93-X-1-31, 94-III-15-175. Tarsometatarsi: NHM A2001 (cast of holotype), A5575 (cast), A5581 (cast). Humerus/Tarsometatarsus: MLP 11-II-20-07.
<i>Palaeudyptes klekowskii</i>	Eocene	Humeri: IB/P/B-0578; MLP 83-I-1-190. Tarsometatarsi: IB/P/B-0065 (holotype), 0551; NHM A5572 (cast).
<i>Palaeudyptes marplei</i>	Late Eocene	Tarsometatarsus: NHM A6119 (cast of holotype).
<i>Palaeospheniscus bergi</i>	Early Miocene	Humerus: MLP 97-VI-1-2. Tarsometatarsi: MLP 20-81 (holotype), 20-414, 97-VI-1-11.
<i>Palaeospheniscus biloculata</i>	Early Miocene	Humeri: AMNH 3346 (holotype), MPEF-PV 1729; MLP 20-565, 77-XII-22-1. Tarsometatarsi: MLP 20-236, 20-415, 97-VI-1-10.
<i>Palaeospheniscus patagonicus</i>	Early Miocene	Humeri: MLP 20-68, 20-530, 20-594, 97-VI-1-1, 97-VI-1-3, 97-VI-1-4; MAC A11047. Tarsometatarsi: MLP 20-34 (holotype), 20-237, 20-240, 97-VI-1-9. Humerus/Tarsometatarsus: MPEF-PV 3069.
<i>Paraptenodytes antarcticus</i>	Early Miocene	Humerus: MLP M619 (cast). Tarsometatarsus: MLP 20-6 (holotype). Humerus/Tarsometatarsus: AMNH 3338.

Table 1 – continued.

Taxon	Epoch	Specimens examined/References for coding
<i>Paraptenodytes brodkorbi</i>	Late Oligocene	Humeri: MAC A11032 (holotype).
<i>Paraptenodytes robustus</i>	Late Oligocene	Humerus: NHM A591 (holotype).
<i>Perudyptes devriesi</i>	Middle Eocene	Humerus/Tarsometatarsus: MUSM 889 (holotype).
<i>Platydyptes amiesi</i>	Late Oligocene	Humerus: Simpson (1971), Ando (2007), photographic record.
<i>Platydyptes marplei</i>	Late Oligocene	Humerus: NHM A4076 (cast of holotype). Tarsometatarsus: Ando (2007).
<i>Platydyptes novaezealandiae</i>	Late Oligocene	Humerus/Tarsometatarsus: Simpson (1971), Ando (2007), photographic record.
<i>Waimanu tuatahi</i>	Late Paleocene	Humerus/Tarsometatarsus: Slack <i>et al.</i> (2006).

(38 taxa, 70 characters); and (iii) the corrected subset including ten additional Paleogene taxa (48 taxa, 70 characters). Finally, in order to explore the position of the newly included taxa, I ran an analysis of the morphological characters (from Chávez Hoffmeister *et al.* 2014) with the corrected humerus/tarsometatarsus subset (48 taxa, 279 characters). All phylogenetic analyses were conducted using TNT 1.1 (Goloboff *et al.* 2003) with a traditional search strategy (10000 replicates of random taxon addition saving 10 trees per replicate, with TBR branch swapping). All characters were equally weighted, multistate coding was used only to represent polymorphism, and branches with a minimum length of zero were collapsed.

The primary sources of the characters are abbreviated as follows. A = Ando (2007); BG = Bertelli and Giannini (2005); C = Clarke *et al.* (2007); CH = Chávez Hoffmeister *et al.* (2014); CL = Clarke *et al.* (2010); LZ = Livezey and Zusi (2006); K = Ksepka *et al.* (2006); KC = Ksepka and Clarke (2010); KF = Ksepka *et al.* (2012); KT = Ksepka and Thomas (2013). Institutional abbreviations (from Table 1): AMNH = American Museum of Natural History, New York, USA; IB/P/B = Institute of Biology, University of Bialystok, Bialystok, Poland; MACN = Museo Argentino de Ciencias Naturales “Bernardino Rivadavia”, Buenos Aires, Argentina; MLP = Museo de La Plata, La Plata, Argentina; MPEF-PV = Museo Paleontológico Egidio Feruglio, Trelew, Argentina; MUSM = Museo de Historia Natural de la Universidad Nacional de San Marcos, Lima, Peru; NHM = Natural History Museum, London, UK.

Character descriptions

Character 1. — Forelimb elements. 0, subcircular in cross section (*Diomedea*); 1, strongly dorsoventrally compressed (*Spheniscus*). Ordered (BG121).

Character 2. — Humerus, head, proximal view, size. 0, moderate (*Diomedea*); 1, enlarged and elliptical (*Gavia*); 2, very enlarged, hemispherical to reniform (*Spheniscus*). New state: The state 1 was previously uncoded. Ordered. (BG122) (Fig. 1A–C)

Character 3. — Humerus, head, proximal view, position respect to the cranio-caudal axis. 0, at midline (*Diomedea*); 1, dorsocaudal (*Kaiika*); 2, caudal (*Spheniscus*). New character: In most birds the humeral head is close to the cranio-caudal axis in proximal view. However, in penguins the head is enlarged and filling most of the dorsal edge in proximal view. This is clearly visible in basal penguins, whereas in crown-ward taxa the head expands over the caudal edge creating a strong reniform shape. Ordered. (Fig. 1A–C)

Character 4. — Humerus, head, dorsal (posterior) view, proximal edge shape. 0, semicircular, with apex located near midline (*Perudyptes*); 1, asymmetric arch with caudal apex, slightly prominent (*Spheniscus*); 2, asymmetric arch with caudal apex, strongly prominent (*Pygoscelis*). (C132) (Fig. 1M–P)

Character 5. — Humerus, head, dorsal (posterior) view, notch between head and dorsal tubercle. 0, present (*Pygoscelis*); 1, absent (*Spheniscus*). (CH157) (Fig. 1M–P)

Character 6. — Humerus, proximal view, accessory pit for ligament insertion adjacent to head. 0, absent or very shallow (*Palaeospheniscus*); 1, deep (*Spheniscus*). (K128) (Fig. 1B–C; Ksepka *et al.* 2006: fig. 8)

Character 7. — Humerus, dorsal tubercle, insertion of minor deltoid muscle. 0, present, deep dorsoproximal groove (*Inkayacu*); 1, inconspicuous to absent (*Spheniscus*). New character: In some stem taxa, a deep groove runs from the dorsal (posterior) surface of the dorsal tubercle to the base of the humeral head over the proximal surface. This groove becomes extremely shallow in crown ward taxa. This character is considered inapplicable in outgroup taxa. (Fig. 1N, P)

Character 8. — Humerus, capital groove, position. 0, caudal (*Anthropornis*); 1, ventrocaudal (*Madrynornis*); 2, ventral (*Spheniscus*). New character: As in most birds, the capital groove is located caudally (ventrally) in basal penguins, being clearly visible in dorsal (caudal) view as a concavity between the head and the edge of the tricipital fossa. The position of the groove becomes more ventral in crown-ward taxa and in most Spheniscidae is mostly ventral, leaving no separation between the head and tricipital fossa in dorsal view. Ordered. (Fig. 1D–F)

Character 9. — Humerus, capital groove, connection with transverse groove. 0, confluent, forming a single (*Kairuku*); 1, connected through a narrow groove (*Palaeospheniscus*); 2, completely separated (*Eudyptula*). (K127) (Fig. 1J–L; Ksepka *et al.* 2006: fig. 10)

Character 10. — Humerus, secondary tricipital fossa, connection with the capital groove. 0, continuous, both structures are undifferentiated (*Perudyptes*); 1, connected, both structures are distinctive (*Inkayacu*); 2, completely separated (*Spheniscus*). New state: The state 1 was previously uncoded. Ordered. (CL222) (Fig. 1M–P)

Character 11. — Humerus, humeral intumescencia, projection from humeral shaft. 0, ventrally projected (*Diomedea*); 1, caudally projected (*Kairuku*); 2, caudoventrally

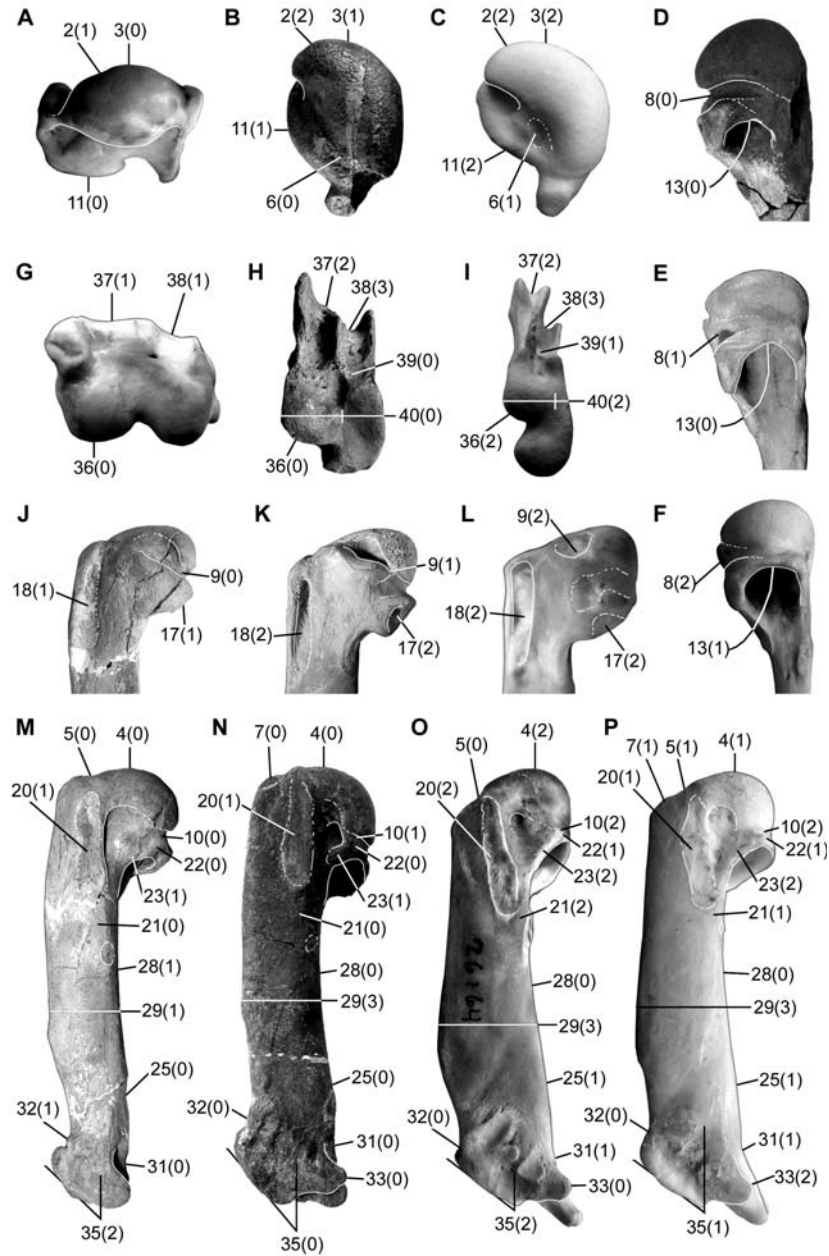


Fig. 1. Humerus characters. Humeri of *Gavia immer* (A), *Anthropornis nordenskjoldi* (B) and *Eudyptes pachyrhynchus* (C), in proximal view; proximal epiphysis of *Palaeudyptes gunnari* (D), *Madrynornis mirandus* (E) and *Spheniscus demersus* (F), in caudal view; *Gavia immer* (G), *Palaeudyptes gunnari* (H) and *Spheniscus magellanicus* (I), in distal view; proximal epiphysis of *Perudyptes devriesi* (J), *Palaeospheniscus patagonicus* (K) and *Eudyptula minor* (L), in ventral view; and *Perudyptes devriesi* (M), *Inkayacu paracasensis* (N), *Pygoscelis adeliae* (O) and *Spheniscus humboldti* (P), in dorsal view. Specimens are not to scale.

projected, being well exposed in cranial view (*Spheniscus*). Modified: K129 define this character based mainly on the orientation of the ventral tubercle, and modified by C135 to refer more specifically to the orientation of the intumescencia, which is used to define the character here. Note that the orientation described for each state is based on the homologous anatomical planes. Ordered. (K129) (Fig. 1A–C; Ksepka *et al.* 2006: fig. 10)

Character 12. — Humerus, tricipital fossa, proximal view, rim. 0, not exposed to slightly exposed at the caudoventral margin (*Palaeospheniscus*); 1, well-exposed along the caudal margin (*Spheniscus*). (K135) (Ksepka *et al.* 2006: fig. 8)

Character 13. — Humerus, tricipital fossa, caudal view, margin. 0, strongly concave (*Madrynornis*); 1, straight to slightly concave (*Spheniscus*). (KT154) (Fig. 1D–F; Ksepka and Thomas 2013: fig. 1m–o)

Character 14. — Humerus, tricipital fossa, developed. 0, shallow, with penetrating pneumatic foramina (*Diomedea*); 1, moderate, without pneumatic foramen (*Gavia*); 2, deep, without pneumatic foramen (*Spheniscus*). (BG123)

Character 15. — Humerus, tricipital fossa. 0, single (*Paraptenodytes*); 1, bipartite (*Palaeospheniscus*). (BG 124) (Bertelli and Giannini 2005: fig. 22)

Character 16. — Humerus, ventral tubercle, dorsal (caudal) view, caudal projection. 0, long, beyond the head (*Waimanu*); 1, short, at level with the head (*Aptenodytes*). New character: In some penguins, the ventral tubercle projects beyond the caudal margin of the humeral head; whereas in others the extension of both structures is subequal. This character is inapplicable in the outgroup.

Character 17. — Humerus, ventral tubercle, tubercle fossa. 0, very shallow, caudal (*Diomedea*); 1, deep, caudal (*Anthropornis*); 2, deep, caudoventral (*Spheniscus*). New character: In many stem penguins the ventral tubercle fossa is located caudally, as in most birds; whereas in crown penguins the fossa is located more caudoventrally, being clearly visible in ventral (cranial) view. (Fig. 1J–L)

Character 18. — Humerus, deltoid crest, cranial coracobrachial muscle scar. 0, superficial, poorly defined scar (*Diomedea*); 1, shallow, well-defined oblong fossa (*Perudyptes*); 2, deep, well-defined oblong fossa (*Spheniscus*). Ordered. (BG125) (Fig. 1J–L)

Character 19. — Humerus, supracoracoideus muscle scar, shape. 0, small and semicircular (*Diomedea*); 1, strongly protruding, greatly elongated over dorsal surface (*Kaiika*); 2, flat, greatly elongated over dorsal surface (*Aptenodytes*). New state: The state 1 was previously uncoded. (K133) (Ksepka *et al.* 2006: fig. 9)

Character 20. — Humerus, supracoracoideus muscle scar, position. 0, attach to dorsal tubercle (*Diomedea*); 1, on shaft dorsal surface, straight to slightly oblique (*Kaiika*); 2, on shaft dorsal surface, strongly oblique (*Pygoscelis*). New character: In penguins, as in *Pelecanoides*, the supracoracoideus scar is expanded and located on the dorsal surface of the humeral shaft. In some stem taxa, the scar is straight and almost parallel to the proximodistal axis of the humerus, whereas in

others like *Pygoscelis*, it is clearly oblique and distally reaches the caudal edge of the humerus. (Fig. 1M–P)

Character 21. — Humerus, supracoracoideus and latissimus dorsi muscle scars, separation. 0, wide gap (*Perudyptes*); 1, moderate gap (*Palaeospheniscus*); 2, small gap or confluent (*Spheniscus*). Ordered. (K134) (Fig. 1M–P; Ksepka *et al.* 2006: fig. 9; Ksepka and Clarke 2010: fig. 26)

Character 22. — Humerus, caudal coracobrachial muscle scar, contact with the distal margin of head. 0, absent (*Diomedea*); 1, present (*Icadyptes*). (CL219) (Fig. 1M–P)

Character 23. — Humerus, caudal coracobrachial muscle attachment. 0, subcircular fossa (*Gavia*); 1, small tubercle (*Kaiika*); 2, flattened wide ovoid scare (*Inkayacu*); 3, flattened narrow elongate scare (*Spheniscus*). New state: The state 1 was previously uncoded. (CL220) (Fig. 1M–P)

Character 24. — Humerus, groove for coracobrachialis nerve. 0, absent or poorly defined (*Spheniscus*); 1, sharp, narrow groove (*Inkayacu*). (CL221)

Character 25. — Humerus, shaft, craniocaudal (dorsoventral) width. 0, shaft thins or maintains width distally (*Pachydyptes*); 1, shaft widens distally (*Spheniscus*). (K136) (Fig. 1M–P; Ksepka *et al.* 2006: fig. 10)

Character 26. — Humerus, nutrient foramen, position. 0, on ventral face of shaft (*Parapterodytes*); 1, on caudal face of shaft (*Apterodytes*). Ordered. (C143)

Character 27. — Humerus, shaft, ventral (anterior) view, elongate furrow along the caudal margin. 0, absent (*Spheniscus*); 1, present (*Icadyptes*). (C144)

Character 28. — Humerus, shaft, ventral (anterior) view, sigmoid curvature. 0, absent or weak (*Parapterodytes*); 1, strong (*Perudyptes*). Note: The degree of curvature is usually more evident at the caudal edge of the shaft. (K137) (Fig. 1M–P; Ksepka *et al.* 2006: fig. 10)

Character 29. — Humerus, shaft, shaft robustness index (proximodistal length/craniocaudal width at middle point). 0, elongated, $SRI \geq 7$ (*Waimanu*); 1, greatly slender, $7 > SRI \geq 6$ (*Perudyptes*); 2, slender, $6 > SRI \geq 5$ (*Palaeudyptes*); 3, thick, $5 > SRI \geq 4$ (*Palaeospheniscus*); 4, bulky, $SRI < 4$ (*Pachydyptes*). Note: For this index, the proximodistal length is measured from the contact between the dorsal tubercle and humeral head (proximal end), to the contact between the ulnar condyle and the trochlear processes (distal end). The craniocaudal (ventrodorsal) width is measured at the middle point of the diaphysis, regardless of the position of the preaxial angle. (CH176) (Figs 1M–P, 3A)

Character 30. — Humerus, dorsal (posterior) view, preaxial angle. 0, absent or inconspicuous (*Madrynornis*); 1, well defined (*Palaeospheniscus*). Note: In state 0, the cranial edge of the shaft is smooth in dorsal view and, in some cases; a weak angle can be identified in ventral view. In contrast, a crest usually demarcates the angle in state 1, which is clearly recognizable in both views. (CH177)

Character 31. — Humerus, dorsal (posterior) view, caudal (ventral) edge, concavity proximal to the dorsal trochlear ridge. 0, present (*Palaeudyptes*); 1, absent (*Spheniscus*). New character: In most basal penguins, a distal concavity separates the proximocaudal margin of the middle and ventral trochlear ridge from the margin of the shaft. The margin is straighter and continuous in more derived taxa, so that part of the middle trochlear ridge only diverges distal to the dorsal ridge. (Fig. 1M–P)

Character 32. — Humerus, dorsal supracondylar tubercle. 0, absent (*Spheniscus*); 1, vestigial, compact tubercle (*Perudyptes*); 2, short process (*Pelecanoides*); 3, elongate process, well expose in distal view (*Puffinus*). New state: The state 2 was previously included in the state 3. (BG126) (Fig. 1M–P)

Character 33. — Humerus, dorsal (posterior) view, dorsal trochlear ridge, projection in relation with the caudal (ventral) margin of the shaft. 0, surpassing it (*Pygoscelis*); 1, reaching the margin (*Palaeospheniscus*); 2, does not reach the margin (*Eretiscus*). Note: In state 1, the ridge slightly exceeds the caudal margin in ventral view but not in dorsal view. (BG128) (Fig. 1N–P; Bertelli and Giannini 2005: fig. 23)

Character 34. — Humerus, brachial muscle scar. 0, cranial ovoid fossa (*Diomedea*); 1, inconspicuous and elongate scar on the cranial margin, between dorsal condyle and preaxial angle (*Spheniscus*); 2, elongate scar on the cranial margin, with deep fossa distal to the preaxial angle (*Palaeudyptes*). (A34) (Ando 2007: figs 3.39, 3.45)

Character 35. — Humerus, angle between main axis of shaft and tangent of dorsal and ventral condyles. 0, less than 30° (*Anthropornis*); 1, 30 to 40° (*Palaeudyptes*); 2, greater than or equal to 40° (*Spheniscus*); 3, nearly 90° (*Diomedea*). Modified: The state ranges have been modified to minimize the use of polymorphic states. The values of angles in all taxa were obtained by photographic analysis using TpsDIG version 2. (K141) (Fig. 1M–P; Ksepka and Clarke 2010: fig. 26)

Character 36. — Humerus, ventral condyle, cranial (dorsal) and distal view. 0, spheroidal, displaced over the ventral (anterior) edge (*Palaeudyptes*); 1, spheroidal, almost parallel to dorsal condyle (*Palaeospheniscus*); 2, flattened, almost parallel to dorsal condyle (*Spheniscus*). (K142) (Fig. 1G–I; Ksepka *et al.* 2006: fig. 11)

Character 37. — Humerus, distal end, humerotricipital groove. 0, absent (*Diomedea*); 1, present (*Pelecanoides*); 2, present, delimited by trochlear ridges (*Waimanu*). New character: The presence of middle and ventral trochlear ridges delimiting the humerotricipital groove is a character shared by all known Sphenisciformes. (Fig. 1G–I)

Character 38. — Humerus, distal end, scapulo-tricipital groove. 0, not demarcated (*Diomedea*); 1, well-marked groove (*Gavia*); 2, well-marked, ventrally delimited by the middle trochlea ridge (*Waimanu*); 3, deep groove, delimited by the dorsal and middle trochlear ridges (*Icadyptes*). New state: The state 2 was previously uncoded. BG defined this character as presence/absence of the distal trochlear ridges, but it was later modified by K139 to refer specifically to the scapulo-tricipital groove ridges. Ordered. (BG127) (Fig. 1G–I)

Character 39. — Humerus, distal view, scapulo- and humerotricipital grooves. 0, separated (*Palaeospheniscus*); 1, cranially connected (*Spheniscus*). New character: In most stem Sphenisciformes, the cranial end of the scapulo- and humerotricipital groove is curved caudally and completely separated from the humerotricipital groove by the intermediate trochlear ridge. In other taxa like *Spheniscus*, the cranial end of the scapulo- and humerotricipital groove is more rectangular and connected to the humerotricipital groove. (Fig. 1H–I)

Character 40. — Humerus, distal view, ratio ventral condyle/adjacent shelf. 0, large, ratio < 1.3 (*Palaeudyptes*); 1, moderate, $1.3 \leq \text{ratio} < 2$ (*Parapterodytes*); 2, greatly reduced, ratio ≥ 2 (*Spheniscus*). Ordered. (K143) (Figs 1H–I, 3B; Ksepka *et al.* 2006 fig. 11)

Character 41. — Tarsometatarsus, elongation index (proximodistal length/medio-lateral width at proximal end). 0, elongated, $\text{EI} \geq 3$ (*Diomedea*); 1, slender, $3 > \text{EI} \geq 2.5$ (*Marambiornis*); 2, shortened, $2.5 > \text{EI} \geq 2$ (*Palaeospheniscus*); 3, greatly shortened, $\text{EI} < 2$ (*Aptenodytes*). Ordered. (BG138) (Fig. 1E–H, 3C)

Character 42. — Tarsometatarsus, proximal view, dorsoplantar compression (maximum lateromedial width/dorsoplantar width at middle point). 0, weak, < 2 (*Waimanu*); 1, strong, ≥ 2 (*Archaeospheniscus*). New character: For this index, the dorsoplantar width at middle point is measured from the intercotylar prominence to the plantar edge of the tarsometatarsus body, excluding the hypotarsal crests. (Figs 2A–D, 3D)

Character 43. — Tarsometatarsus, proximal view, size of cotylae. 0, lateral bigger than medial (*Gavia*); 1, subequal (*Spheniscus*); 2, medial bigger than lateral (*Eudyptula*). New character: In most penguins both cotylae are subequal in size, with the medial cotyla slightly larger than the lateral; however, in some taxa like *Aptenodytes* and *Eudyptula* the medial cotyla is much bigger than the lateral, whereas in *Gavia* the lateral cotyla is the biggest one. (Fig. 2A–D)

Character 44. — Tarsometatarsus, lateral cotyla, dorsomedially expanded. 0, absent (*Anthropornis*); 1, present (*Palaeospheniscus*). New character: In some taxa the dorsal edge of the lateral cotyla is dorsomedially deflected, expanding it slightly under the intercotylar prominence. (Fig. 2A–C)

Character 45. — Tarsometatarsus, lateral cotyla dorsal view, lateral projection. 0, prominent (*Waimanu*); 1, flattened (*Palaeospheniscus*). New character: In most birds the lateral cotyla projects well-beyond the lateral edge of the tarsometatarsus body, something that can also be seen in *Waimanu*. In contrast, in most penguins the cotyla is flatter so that rarely exceed the lateral edge of the body. (Fig. 2E–H)

Character 46. — Tarsometatarsus, medial cotyla, proximal view, pointed dorsal edge. 0, absent (*Pygoscelis*); 1, present (*Spheniscus*). New character: In some penguins like *Spheniscus* the dorsal edge of the medial cotyla is pointed, creating a slightly hooked margin. (Fig. 2A–D)

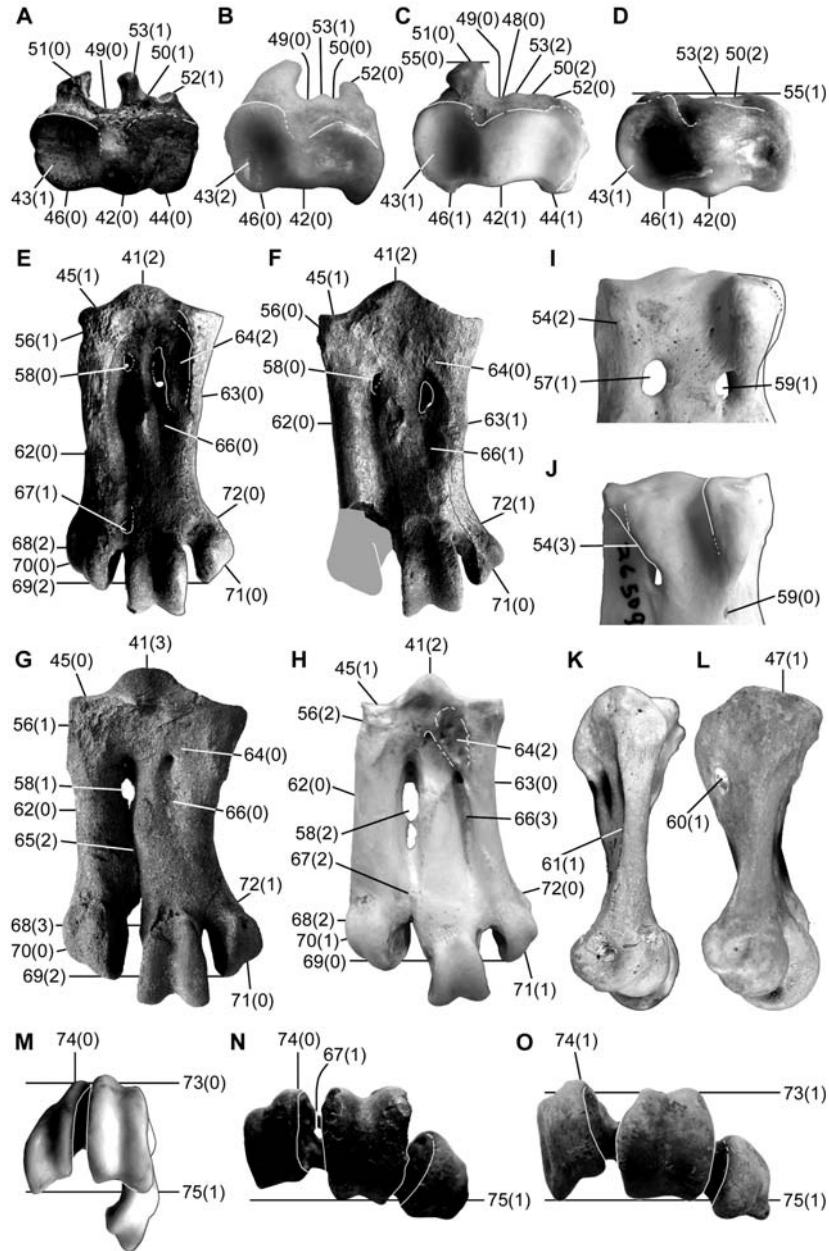


Fig. 2. Tarsometatarsus characters. Tarsometatarsus of *Marambiornis exilis* (A), *Eudyptula minor* (B), *Spheniscus demersus* (C) and *Pygoscelis antarcticus* (D), in proximal view; *Delphinornis larseni* (E), *Anthropornis grandis* (F), *Palaeudyptes klekowskii* (G) and *Spheniscus magellanicus* (H), in dorsal view; proximal end of *Aptenodytes forsteri* (I) and *Eudyptes pachyrhynchus* (J), in plantar view; *Palaeospheniscus patagonicus* (K) in lateral view; *Madrynornis mirandus* (L) in medial view; and *Gavia immer* (M), *Delphinornis larseni* (N) and *Spheniscus megaramphus* (O), in distal view. Specimens are not to scale.

Character 47. — Tarsometatarsus, medial cotyla, position. 0, proximal (*Paraptenodytes*); 1, slightly dorsodistally deflected (*Pygoscelis*); 2, strongly dorsodistally deflected (*Spheniscus*). New character: The medial cotyla in most penguins is dorsodistally deflected, forming a sloped edge in medial view. When this deflection is strong, the interior of the cotyla is clearly visible in dorsal view. The cotyla can also be proximally located, forming an almost straight proximal edge in medial view. (Fig. 2L)

Character 48. — Tarsometatarsus, proximal view, enclosed hypotarsal canal for superficial flexor tendons. 0, absent (*Waimanu*); 1, present (*Gavia*). Modified: BG defined this character as presence/absence of any hypotarsal canals. Here this character is only use for the enlarged hypotarsal canal present in *Gavia*, whereas other canals are treated as separate characters (see Characters 49 and 50). Ordered. (BG141) (Fig. 2C)

Character 49. — Tarsometatarsus, proximal view, tendon of muscle flexor digitorum longus. 0, groove (*Waimanu*); 1, partially closed groove (*Diomedea*); 2, canal (*Puffinus*). New character: The tendon of muscle flexor digitorum longus runs through a groove in all known Sphenisciformes. In Procellariiformes the groove can be partially closed as in *Gavia*, or fully closed and forming a canal. (Fig. 2A–C)

Character 50. — Tarsometatarsus, proximal view, tendon of muscle flexor hallucis longus. 0, groove, delimited by a lateral and intermediate crest (*Gavia*); 1, groove, laterally open (*Waimanu*); 2, inconspicuous or absent (*Palaeospheniscus*); 3, canal (*Puffinus*). New character: In Gaviiformes, the tendon of muscle flexor hallucis longus runs through a well-defined groove between the lateral and intermediate hypotarsal crests. In most Procellariiformes it forms a canal, whereas in *Diomedea* it is located in a shallow but well-defined groove. In basal penguins like *Marambiornis*, the tendon runs through a laterally open groove, limited by a high intermediate crest and a very short lateral crest. Nevertheless, in most penguins this groove is completely absent or vestigial. (Fig. 2A–D)

Character 51. — Tarsometatarsus, medial hypotarsal crest. 0, present (*Spheniscus*); 1, absent (*Kairuku*). (KF243) (Fig. 2A–C; Ksepka *et al.* 2012: fig. 71, p, r)

Character 52. — Tarsometatarsus, medial hypotarsal crest, proximal view, bilobulated. 0, absent (*Spheniscus*); 1, present (*Paraptenodytes*). New character: In some fossil penguins, the medial crest develops a well-defined lateral ridge separated from the shorter medial edge; whereas in most penguins the crest is monolobulated. (Fig. 2A–C)

Character 53. — Tarsometatarsus, intermediate hypotarsal crest. 0, two well-defined crests (*Oceanodroma*); 1, one well-defined crest (*Marambiornis*); 2, indistinguishable from lateral crest or absent (*Spheniscus*). New state: The state 0 was previously uncoded. In penguins, the intermediate crest is usually connected to the lateral crest. For this character, the number of intermediate crests is counted re-

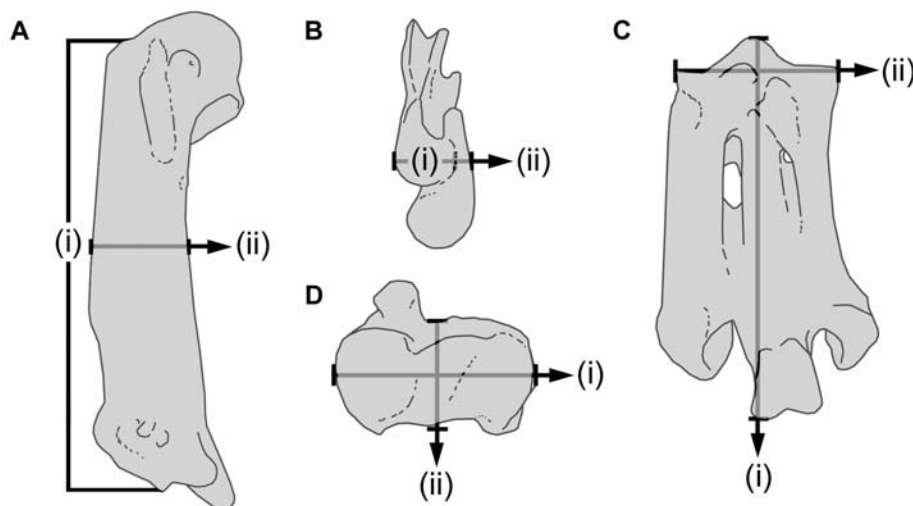


Fig. 3. Measurement points for continuous characters. All indices were calculated as (i)/(ii). Measurements for Character 29, shaft robustness index (A); Character 40, ratio ventral condyle/adjacent shelf (B); Character 41, elongation index (C); and Character 42, dorsoplantar compression (D).

ardless if they delimited grooves or are plantarly connected with other crests and forming canals. Ordered. (K158) (Fig. 2A–D; Ksepka *et al.* 2006: figs 14–15)

Character 54. — Tarsometatarsus, lateral hypotarsal crest, plantar view. 0, enlarged and connected with medial crest (*Gavia*); 1, well defined and parallel to proximodistal axis of tarsometatarsus (*Diomedea*); 2, reduced, poorly defined and proximal to lateral foramen (*Pygoscelis*); 3, forming a diagonal ridge that overhangs lateral foramen (*Palaeospheniscus*). (CH224) (Fig. 2I–J)

Character 55. — Tarsometatarsus, proximal view, lateral hypotarsal crest, plantar projection relative to medial hypotarsal crest. 0, shorter (*Spheniscus*); 1, subequal (*Pygoscelis*). (KT203) (Fig. 2C–D)

Character 56. — Tarsometatarsus, collateral lateral ligament scar. 0, absent or inconspicuous (*Anthropornis*); 1, well defined, creating a depression over the lateral surface (*Inkayacu*); 2, well defined, creating a notch on the proximolateral vertex (*Paraptenodytes*). (CH219) (Fig. 2E–H)

Character 57. — Tarsometatarsus, proximal vascular foramina, plantar view. 0, medial foramen present, lateral foramen absent or vestigial (*Anthropornis*); 1, both foramina present (*Spheniscus*); 2, lateral foramen present, medial foramen absent or vestigial (*Palaeospheniscus*). Note: State 1 refers to the plantar opening of the medial foramen; regardless if it is open at the plantar surface as in *Pygoscelis*, or at the medial surface of the medial hypotarsal crest as in *Spheniscus*. (K162) (Fig. 2I; Ksepka *et al.* 2006: figs 14–15; Ksepka and Clarke 2010: fig. 30)

Character 58. — Tarsometatarsus, lateral foramen, dorsal view. 0, absent or vestigial (*Eretiscus*); 1, small (*Pygoscelis*); 2, enlarged (*Spheniscus*). Note: Although

there is a large quantitative variation in the size of the vascular foramina, the extreme morphologies described for states 0 and 2 are exclusive of some taxa. (CH229) (Fig. 2E–H)

Character 59. — Tarsometatarsus, medial foramen, plantar view, opens distally to medial crest. 0, absent (*Spheniscus*); 1, present (*Aptenodytes*). (BG140) (Fig. 2I–J)

Character 60. — Tarsometatarsus, medial foramen, medial view, perforating the medial hypotarsal crest. 0, absent (*Pygoscelis*); 1, present (*Spheniscus*). (BG139) (Fig. 2L; Bertelli and Giannini 2005: fig. 26)

Character 61. — Tarsometatarsus, lateral edge, lateral view, strongly dorsoplantarly compressed. 0, absent (*Spheniscus*); 1, present (*Palaeospheniscus*). New character: In some penguins, the lateral edge of the metatarsal IV is strongly compressed creating a distinctive sharp edge; but in most of them, it is subcylindrical or with a slightly flattened plantar surface. (Fig. 2K)

Character 62. — Tarsometatarsus, lateral edge, dorsal view. 0, straight (*Palaeospheniscus*); 1, concave (*Eretiscus*). Note: This character only refers to the edge of the lateral metatarsal, whereas the degree of projection of the trochlea and cotyla are treated as independent characters (see Characters 45 and 70). In most penguins the lateral edge of the tarsometatarsus is straight; however in some fossil taxa like *Eretiscus* the edge is concave. (A72) (Fig. 2E–H)

Character 63. — Tarsometatarsus, dorsal view, medial margin, pronounced convexity. 0, absent (*Palaeudyptes*); 1, present (*Anthropornis*). (K157) (Fig. 2E–H)

Character 64. — Tarsometatarsus, dorsal view, medial infracotylar groove. 0, absent or poorly defined (*Anthropornis*); 1, present, proximal to the medial foramen (*Pygoscelis*); 2, present, overhanging the medial foramen (*Spheniscus*). New character: The medial infracotylar groove is usually poorly differentiated in giant Eocene penguins, but it became a more distinctive structure in other taxa. In penguins like *Pygoscelis*, this groove can be laterally open or limited by shallow tuberosities; whereas in others like *Spheniscus*, it is laterally delimited by a crest or lamina that overhangs and partially occludes the foramen. (Fig. 2E–H)

Character 65. — Tarsometatarsus, dorsal view, lateral dorsal groove. 0, absent or poorly defined (*Diomedea*); 1, present, distal (*Gavia*); 2, present, along all the body (*Anthropornis*). New character: In most birds the lateral dorsal groove is medially open and poorly defined, or only well-defined distally in association with the distal vascular foramen. In penguins, the groove is always well defined along the length of the tarsometatarsus. (Fig. 2G)

Character 66. — Tarsometatarsus, dorsal view, medial dorsal groove. 0, absent or barely perceptible (*Delphinornis*); 1, shallow groove (*Palaeospheniscus*); 2, moderate groove (*Eudyptes*); 3, deep groove (*Spheniscus*). Ordered. (K159) (Fig. 2E–H; Ksepka *et al.* 2006: fig. 15)

Character 67. — Tarsometatarsus, distal vascular foramen. 0, present, one plantar opening, over the lateral intertrochlear notch (*Waimanu*); 1, present, two plantar

openings, one over and one on the lateral intertrochlear notch (*Mesetaornis*); 2, absent (*Spheniscus*). Modified: K defined the state 1 only as “open distally” and scored it as present only in *Mesetaornis* and *Marambiornis*. However, a plantar opening is also present in *Mesetaornis*, as well as in *Delphinornis arctowskii* and *D. larseni* (IB/P/B-0062). Unfortunately the state of this character cannot be verified in *Marambiornis* and other species of *Delphinornis*, in which one or two openings can be present. Ordered. (K163) (Fig. 2E, H, N; Ksepka *et al.* 2006: fig. 15; Ksepka and Clarke 2010: fig. 30)

Character 68. — Tarsometatarsus, intertrochlear notches, dorsal view. 0, medial notch absent (*Gavia*); 1, medial notch deeper than lateral (*Puffinus*); 2, subequal (*Waimanu*); 3, lateral notch deeper than medial (*Madrynornis*). (CH233) (Fig. 2E–H)

Character 69. — Tarsometatarsus, medial and lateral trochleae, dorsal view. 0, medial trochlea shorter than lateral (*Gavia*); 1, lateral trochlea slightly shorter than medial (*Inkayacu*); 2, subequal (*Palaeospheniscus*). (CH234) (Fig. 2E–H)

Character 70. — Tarsometatarsus, lateral trochlea, dorsal view. 0, laterally projected (*Waimanu*); 1, straight (*Spheniscus*); 2, medially deflected (*Archaeospheniscus*). (K160) (Fig. 2E–H)

Character 71. — Tarsometatarsus, medial trochlea, dorsal view, medial projection. 0, strongly projected (*Mesetaornis*); 1, moderately projected (*Kairuku*); 2, plantolaterally deflected (*Gavia*). New character: In most stem penguins the medial trochlea projects far beyond the medial edge of the tarsometatarsus body, which is aligned with the medial edge of the medial trochlea as in most Procellariiformes. In contrast, the trochlea is located closer to the body in most crown-ward taxa and strongly plantolaterally deflected in Gaviiformes. (Fig. 2E–H)

Character 72. — Tarsometatarsus, medial trochlea, dorsal view, presence of a neck between the trochlea and the tarsometatarsus body. 0, absent (*Aptenodytes*); 1, present (*Inkayacu*). New character: In some stem penguins, the medial trochlea is separated from the tarsometatarsus body, developing a neck-like structure that connects it to the body. In other penguins and outgroup taxa, the trochlea is in direct contact with the body. (Fig. 2E–H)

Character 73. — Tarsometatarsus, lateral trochlea, distal view. 0, dorsally aligned with intermediate trochlea (*Palaeodyptes*); 1, dorsally deflected (*Delphinornis*); 2, plantarly deflected (*Diomedea*). New state: The state 2 was previously uncoded. (KT211) (Fig. 2M, O; Ksepka and Thomas 2013: fig. 1w–y)

Character 74. — Tarsometatarsus, lateral trochlea, distal view, laterally deflected. 0, absent (*Palaeospheniscus*); 1, present (*Megadyptes*). Note: In some penguins the lateral trochlea is strongly laterally deflected giving a triangular shape to the intertrochlear incisure in distal view. In this state, the medial surface of the lateral trochlea is clearly visible in dorsal view. (LZ2366) (Fig. 2M–O)

Character 75. — Tarsometatarsus, medial trochlea, distal view, strongly plantarly deflected. 0, absent (*Pygoscelis*); 1, present (*Kairuku*). Note: This character refers

to the plantar edge of the medial trochlea with respect to the plane defined by the most plantar point of the intermediate and lateral trochleae in distal view; or with respect to the plane defined by the trochlear ridges of the intermediate trochlea when the lateral trochlea is strongly dorsally deflected. (A73) (Fig. 2M–O)

Phylogenetic analysis

Humerus/Tarsometatarsus-only. — As could be expected for the analyses limited to subsets of characters, the resolution of the strict consensus for all the tested sets (Fig. 4) is poorer than that in former analyses based on the full morphological dataset or its combination with molecular data (*e.g.*, Ksepka *et al.* 2012; Ksepka and Thomas 2013). The uncorrected subset of Chávez Hoffmeister *et al.* (2014) results in 18 most parsimonious trees (MPTs) (153 steps) (Fig. 4A), less than using the corrected subset with an equivalent sample of taxa (772 MPTs, 279 steps) (Fig. 4B) or with the additional taxa (5430 MPTs, 303 steps) (Fig. 4C). Under an equivalent sample of taxa, the uncorrected subset also recovers a better solved topology than the corrected subset. This difference in the performance of both versions is mainly attributed to the correction of states coding in the new set, which introduced polymorphic states in several taxa. As a result, some of the previous synapomorphies became ambiguous, decreasing the overall resolution of the subset when a reduced sample of taxa is used. Despite this difference several internal nodes are recovered and the general polarity seems to be congruent between both sets and with previous analyses. Additionally, the resolution of some nodes is improved with the inclusion of additional taxa (Fig. 4C), particularly *Palaeudyptes marplei* and the *Hakataramea* penguin.

Apart from the differences in resolution of trees, the general topology derived from both datasets is mostly congruent when equivalent taxa are used. Nevertheless, there is a disagreement regarding the monophyly of *Delphinornis*. The corrected dataset suggests that *Delphinornis* is a polyphyletic genus, with *D. gracilis* more closely related to *Mesetaornis* and *Marambiornis*, and *D. arctowskii* separated from the type species *D. larseni* (Fig. 4B). This part of the tree collapses with the inclusion of *Crossvallia* and *Kaiika* (Fig. 4C). Additionally, *Madrynornis* is excluded from the crown group, partially improving the internal polarity of the clade.

On the other hand, some important differences (regarding the topology in comparison with previous analyses) appear with the inclusion of the additional taxa (Fig. 4C). One of the main differences is the recovery of a monophyletic clade composed of *Kairuku*, *Palaeudyptes*, *Inkayacu*, *Pachydyptes* and the Burnside “*Palaeudyptes*”. *Kairuku* is recovered as a monophyletic genus at the base of the clade, whereas *Palaeudyptes antarcticus* appears in a polytomy with *Pachydyptes* and the Burnside “*Palaeudyptes*”. The most internal clade comprises the

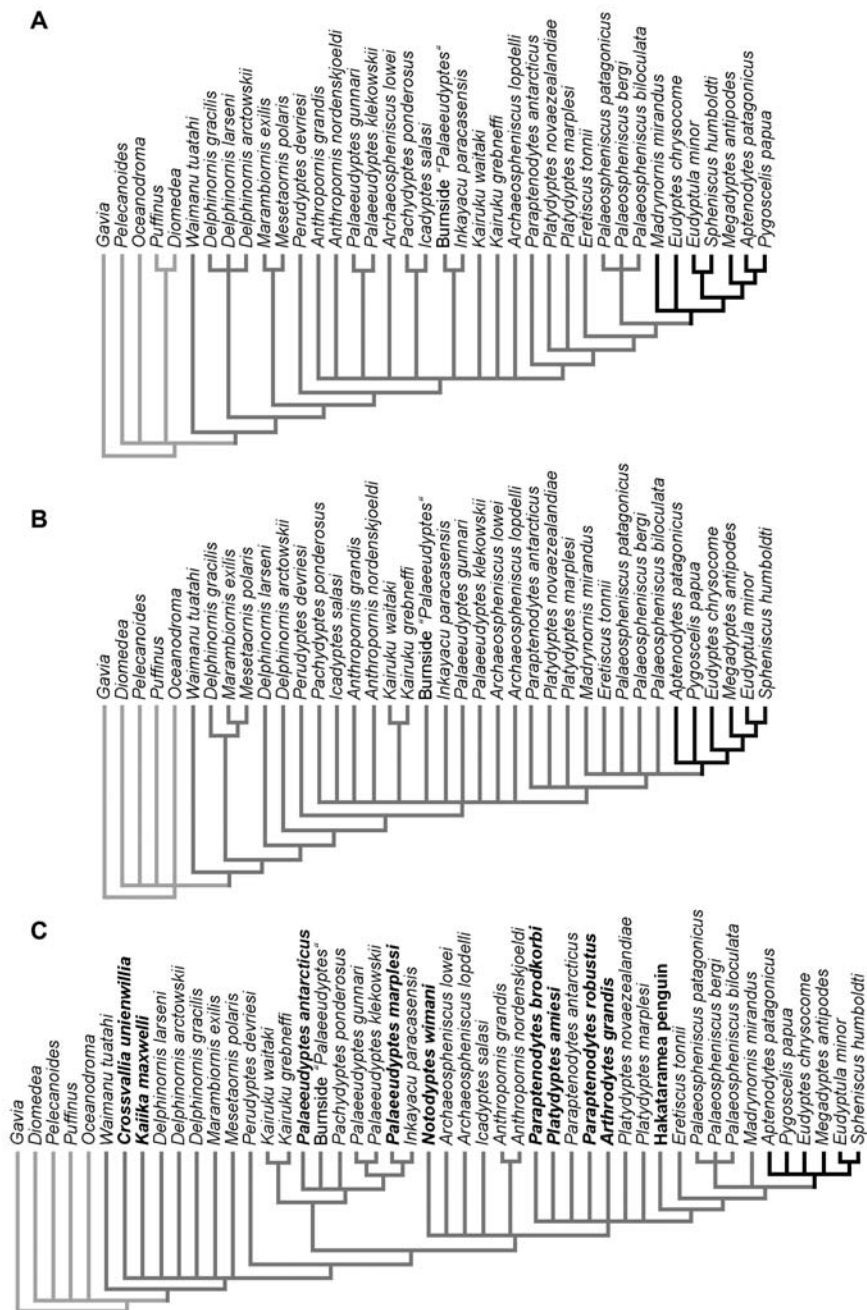


Fig. 4. Strict consensus resulting from the analysis of humerus and tarsometatarsus characters. **A.** Uncorrected subset (38 taxa, 50 characters, 18 MPTs, 153 steps) from Chávez Hoffmeister *et al.* (2014). **B.** Corrected subset with an equivalent sample of taxa (38 taxa, 70 characters, 772 MPTs, 279 steps). **C.** Corrected subset including 10 new taxa (48 taxa, 70 characters, 5430 MPTs, 303 steps).

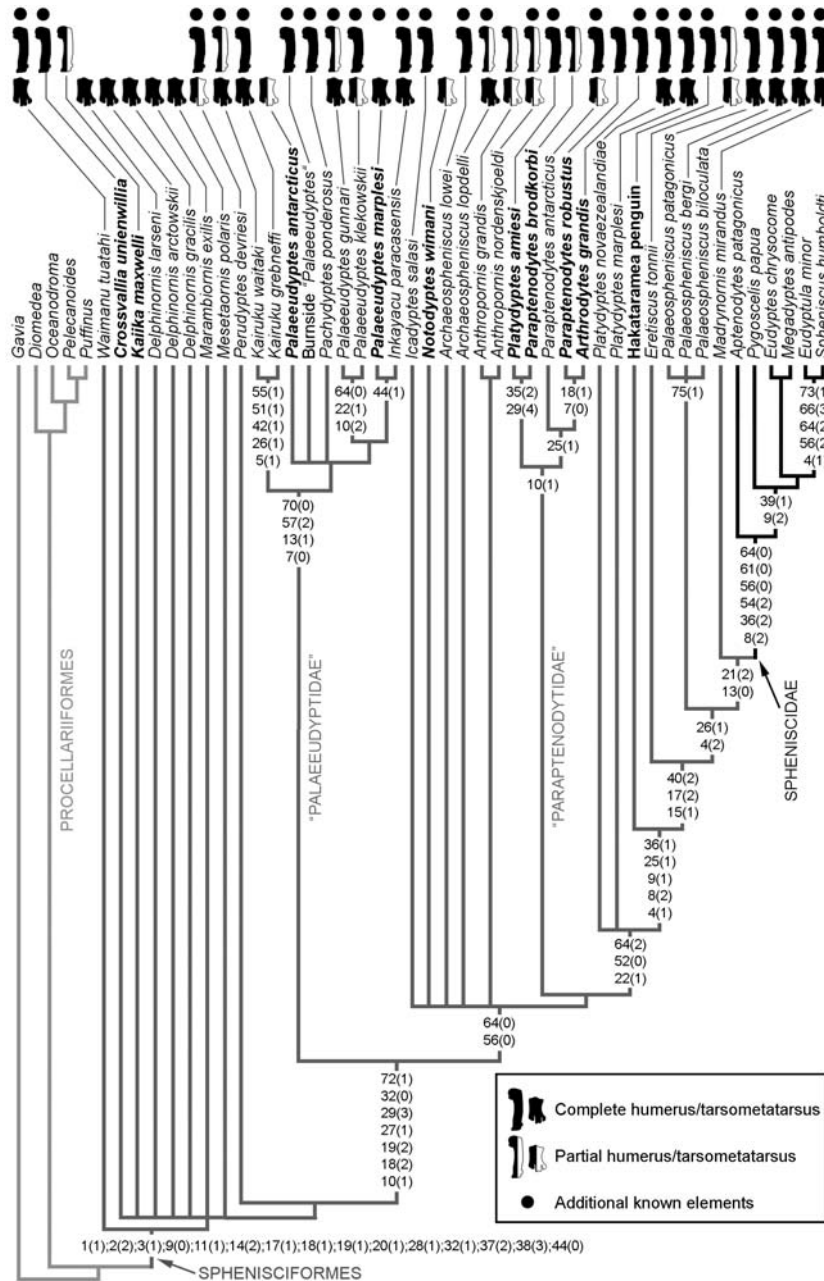


Fig. 5. Strict consensus tree of 769 MPTs (706 steps) resulting from an analysis of morphological-only characters (Chávez Hoffmeister *et al.* 2014) with correction of the humerus-tarsometatarsus subset. Humeral and tarsometatarsal synapomorphies shared across all trees are listed for each main node using the numeration from the current paper. Known elements and their completeness are illustrated for each fossil taxon. Completeness refers to how much is known about each element, so that multiple specimens can be considered when available. Quality of preservation is not illustrated.

Table 2
Osteological synapomorphies for main clades based on the corrected morphological characters from Chávez Hoffmeister *et al.* (2014). Humeral and tarsometatarsal synapomorphies are listed in Fig. 5. Numeration based on Chávez Hoffmeister *et al.* (2014).

Clade	Synapomorphies
Sphenisciformes	(89:2) Skull, temporal fossa greatly deepened
“Palaeudyptidae”	(216:0) Tibiotarsus, lateral sulcus extensorius
<i>Madrynornis</i> + Spheniscidae	(143:1) Scapula, facies articularis humeralis compressed and ovoid (207:0) Pelvis, foramen ilioischadicum smaller or similar in size to foramen acetabuli
Spheniscidae	(77:0) Rostrum, visible naso-premaxillary suture (105:1) Quadrate, tubercle form. adductor mandibulae externus present as a ridge (136:0) Sternum, sulcus articularis coracoideus essentially straight (147:1) Coracoid, shallow scapular cotyle

two Antarctic species attributed to *Palaeudyptes*, *P. gunnari* and *P. klekowskii*, joined as the sister clade to the one including *P. marplei* and *Inkayacu*. A second important difference relates to the position of *Anthropornis* and *Notodyptes*. Both taxa appear in a more derived position than in previous analyses, within a polytomy that also includes *Icadyptes* and *Archaeospheniscus*.

Corrected morphological matrix. — The analysis of the corrected dataset of Chávez Hoffmeister *et al.* (2014) results in 769 MPTs of 706 steps (Fig. 5). The performance and resolution of the strict consensus show a considerable improvement in comparison with the analysis based on the subset of characters, but with a poorer resolution than that achieved by the former full-morphology analyses regarding the basal taxa and the monophyly of several genera (*e.g.*, Ksepka *et al.* 2012; Chávez Hoffmeister *et al.* 2014). However, the relations among more derived taxa are well solved. Two large polytomies are recovered: one at the base of the tree including *Crossvallia*, *Kaiika*, *Delphinornis*, *Marambiornis* and *Mesetaornis*; and one in a more derived node including *Icadyptes*, *Notodyptes*, *Archaeospheniscus* and *Anthropornis*. Additionally, only three non-monotypic genera have been recovered as monophyletic: *Kairuku*, *Anthropornis* and *Palaeospheniscus*. Nevertheless, several internal nodes are recovered, including the crown Spheniscidae and two new clades of stem taxa. Additionally, the internal topology and polarity of Procellariiformes and Spheniscidae are largely congruent respect to studies based on combined data (*e.g.*, Ksepka and Thomas 2013; Ksepka *et al.* 2012).

The topology shows some important differences with respect to former studies based on morphological data (Ksepka *et al.* 2012; Chávez Hoffmeister *et al.* 2014). As in the corrected subset of humerus/tarsometatarsus characters (Fig. 4C), an identical clade composed of *Kairuku*, *Palaeudyptes*, *Inkayacu*, *Pachydyptes* and the Burnside “*Palaeudyptes*” is recovered. This is due to the fact that most of the synapomorphies of this clade are humerus/tarsometatarsus characters (see Table 2 and Fig. 5). Similarly, the position of *Anthropornis* and *Notodyptes* is also identical

to that recovered from the corrected subset. Furthermore, a second monophyletic clade composed of *Paraptenodytes*, *Arthrodytes* and *Platydyptes amiesi* is recovered. *Platydyptes amiesi* and *Paraptenodytes brodkorbi* are joined at the base of the clade, whereas *P. antarcticus* appears as the sister taxon of the clade comprising *P. robustus* and *Arthrodytes*. This clade is supported by humerus/tarsometatarsus synapomorphies, but is only recovered in the majority-rule consensus of the corrected subset, with the same internal nodes recovered in 73 to 88% of the trees. Finally, *Platydyptes novaezealandiae* and *P. marplei* are recovered in a more derived node, whereas the Hakataramea penguin, *Eretiscus*, *Palaeospheniscus* and *Madrynormis* are arranged in a series leading to crown Spheniscidae.

Discussion and final remarks

The purpose of the present revision is to improve the scope and coverage of the phylogenetic characters in two key skeletal elements of penguins, the humerus and tarsometatarsus, but the resulting dataset has been intended as a correction of the morphological matrix proposed by Chávez Hoffmeister *et al.* (2014), and not as an independent matrix. As has been noted by other authors (Bertelli *et al.* 2006; Ksepka and Clarke 2010), and regardless of the potential increase in the percentage of missing data for some fossil taxa, the use of subsets of characters is likely to reduce the accuracy of the analysis in comparison with the full dataset. This is evidenced here in the low resolution of the strict consensus derived from the subset (Fig. 4C) compared with the complete dataset (Fig. 5). However, if we compare its majority-rule consensus with the full-morphology strict consensus, it is clear that the topology of both trees is very similar. This is because most of the stem nodes recovered with the full morphological matrix are supported by humeral and tarsometatarsal synapomorphies, whereas other elements like the skull become more important to define Sphenisciformes and Spheniscidae (see Table 2 and Fig. 5). This in turn is related to the strong “type-element” bias among fossil penguins, for which at least one of these two elements is known, but additional equivalent elements are relatively rarer. Nevertheless, it is clear that the use of the complete dataset improves the performance of the analysis, improving the polarity and introducing additional informative characters. A good example of this can be seen within Spheniscidae, where for the first time the rooting is in agreement with that obtained in molecular and combined analyses (Ksepka *et al.* 2012; Subramanian *et al.* 2013; Chávez Hoffmeister *et al.* 2014).

The present analysis has also been intended as a means to explore the relations of several previously excluded Paleogene taxa, and some of those poorly represented in the fossil record, like *Palaeudyptes antarcticus* and *Notodyptes wimani*, which may need to be excluded in more extensive analyses. Most of them fall close to their expected positions (Ksepka and Clarke 2010). The early penguins *Cross-*

vallia and *Kaiika* are placed close to the base of the tree. It is important to mention that during the preliminary analysis, the exclusion of both taxa increases the resolution of the base of the tree, which later collapses due to the lack of comparable elements in *Delphinornis*, *Mesetaornis* and *Marambiornis* (Fig. 5); however, it also helps to improve the polarity of the humeral characters. In contrast, the exclusion of the remaining taxa reduces the resolution of the strict consensus, being identified as informative taxa despite the limited specimens available for many of them.

The corrected morphological matrix has given rise to some interesting questions regarding the relationships among Paleogene penguins, particularly concerning the possible existence of extinct clades. Nodes including many Late Eocene taxa, and *Palaeudyptes* in particular, were often collapsed (Ksepka and Clarke 2010; Ksepka *et al.* 2012) or arranged in a gradient (Chávez Hoffmeister *et al.* 2014) in former morphological analyses. This analysis recovers for the first time a monophyletic clade containing *Palaeudyptes* and its closest relatives, reminiscent of the “Palaeudyptinae” subfamily proposed by Simpson (1946) based on the morphology of the same elements corrected here. The internal topology of this clade supports the monophyly of *Kairuku*, as well as the sister relationship between the Antarctic species of *Palaeudyptes* and the clade *P. marplei* + *Inkayacu*. This confirms the close relation between *Inkayacu* and the Antarctic *Palaeudyptes* (Jadwiszczak 2011), and may even imply that *Inkayacu* could be a junior synonym of *Palaeudyptes*. Unfortunately, because the position of *Palaeudyptes antarcticus* is unresolved, the monophyly of this genus cannot be confirmed. Interestingly, *Pachydyptes* is also included in this clade, whereas the most recent proposal suggested a closer relation with *Icadyptes* (Chávez Hoffmeister *et al.* 2014).

A clade containing *Paraptenodytes* and its closest relatives, equivalent to the “Paraptenodytinae” subfamily of Simpson (1946), is also recovered. *Paraptenodytes antarcticus* is the only taxon included in previous analyses recovered as part of this clade, which mostly contains Late Oligocene species from Argentina. Unfortunately, most of these newly added taxa are represented by isolated and fragmentary humeri, namely *Arthrodytes* and *Platydyptes amiesi* are the only ones with additional elements available for comparison. Acosta Hospitaleche (2005) considered *Paraptenodytes brodkorbi* as a junior synonym of *P. robustus*; however, after examining the type specimens of both species, I consider them as separate taxa and agree with Bertelli *et al.* (2006) that they may belong to different genera. This is in agreement with the results of the phylogenetic analysis of the corrected full morphological dataset, where *P. brodkorbi* is recovered as the sister taxon of *Platydyptes amiesi* from the Late Oligocene of New Zealand, suggesting that both genera may be paraphyletic. It is important to note, that despite the existence of partial skeletons attributable to *P. amiesi* (Ando 2007), only the type humerus and radius were considered in the present analysis. On the other hand, *Paraptenodytes robustus* and *Arthrodytes* are joined by two humeral synapomorphies absent in *P. antarcticus*: (i)

deep dorsoproximal insertion of minor deltoid muscle on dorsal tubercle (Character 7:0), and (ii) shallow coracobrachial muscle fossa (Character 18:1). This suggests that *P. robustus* could be in fact a species of *Arthrodytes*, in which case *Parapterodytes* may represent a monotypic genus.

Another interesting issue is the position of *Anthropornis*. This genus has been recovered mostly in a basal node between *Perudyptes* and the “Late Eocene–Palaeoedyptes” assemblage (e.g., Ksepka and Clarke 2010; Ksepka *et al.* 2012; Chávez Hoffmeister *et al.* 2014). Here it is recovered in a more derived position and in closer relation with *Icadyptes*, *Archaeospheniscus* and *Notodyptes*. A comparison of several arrangements during the preliminary analyses suggests that the inclusion of *Notodyptes wimani* is the main cause of this change. Based only on its morphology, Simpson (1971) synonymized this Antarctic genus with *Archaeospheniscus* Marples, 1952 from New Zealand, an arrangement later validated by Myrcha *et al.* (2002). However, Ksepka and Clarke (2010) reassigned the species to the genus *Delphinornis* based on their phylogenetic analysis, for which they used only bibliographic data for the coding of this species. Recently, Jadwiszczak (2013) questioned this interpretation, based on a phylogenetic analysis of tarsometatarsus characters with a reduced taxonomic sample. Interestingly, *Notodyptes* is here recovered in the same collapsed node as *Archaeospheniscus* (Fig. 5), being more congruent with the interpretations of Simpson (1971) and Myrcha *et al.* (2002). Three tarsometatarsal synapomorphies support the position of *Notodyptes* and its separation from *Delphinornis*: (i) absence of a collateral lateral ligament scar (Character 56:0), (ii) absence of the medial infracotylar groove (Character 64:0), and (iii) presence of a neck between the medial trochlea and the tarsometatarsus body (Character 72:1). Considering these results, along with the morphological differences noticed by other authors (e.g., Simpson 1971, Myrcha *et al.* 2002) and myself during the revision of the type specimens, I strongly recommend the exclusion of this species from *Delphinornis*. Nevertheless, it is important to notice that the inclusion of the species in *Archaeospheniscus* is not supported by the present analysis, and that the position of this taxon is likely to remain unresolved without the discovery of better preserved specimens. In this context, I recommend the provisional use of the original denomination for this taxon: *Notodyptes wimani*.

It is clear that the humerus and tarsometatarsus are key elements for the study of the evolution of penguins (Walsh *et al.* 2007, 2008), providing several informative characters in a phylogenetic context. This is accentuated by the “type-element” bias among fossil penguins. In this context, an accurate representation of the humerus/tarsometatarsus characters and states is essential to improve our understanding of their early evolution. A meticulous revision of the remaining morphological characters will be crucial to test some aspects of the new arrangement introduced by this corrected dataset, particularly considering the existence of additional elements for several of the taxa here included.

Acknowledgments. — I would like to thank Peter Capainolo, Paul Sweet, Lydia Garetano, Carl Mehling and Joel Cracraft (American Museum of Natural History, USA), Piotr Jadwiszczak (Uniwersytet w Białymstoku, Poland), Rodolfo Salas (Museo de Historia Natural de la Universidad Nacional de San Marcos, Peru), Marcelo Reguero (Museo de La Plata, Argentina), Alejandro Kramarz (Museo Argentino de Ciencias Naturales, Argentina), Diego Pol (Museo Paleontológico Egidio Feruglio, Argentina), Sylke Frahnert and Pascal Eckhoff (Museum für Naturkunde, Germany), Bob McGowan and Stig Walsh (National Museum of Scotland, UK) and Sandra Chapman (Natural History Museum, UK) for facilitating access to important comparative specimens. Special thanks are given to the Division of Ornithology Collection Study Grant of the AMNH and the Palaeobiology Research Group Bob Savage Memorial Fund of the University of Bristol, which provided financial support for my visits to the collections of the American Museum of Natural History and Uniwersytet w Białymstoku respectively. Roberto Yury Yáñez (Universidad de Chile, Chile) and an anonymous reviewer helped to improve this paper during the submission processes. I also want to thank Michael Benton (University of Bristol, UK) and Daniel Ksepka (North Carolina State University, USA) for their support.

References

- ACOSTA HOSPITALECHE C. 2005. Systematic revision of *Arthrodytes* Ameghino, 1905 (Aves, Spheniscidae) and its assignment to the Paraptendyinae. *Neues Jahrbuch für Geologie und Paläontologie* 7: 404–414.
- ACOSTA HOSPITALECHE C., TAMBUSI C. and COZZUOL M. 2004. *Eretiscus tonnii* (Simpson) (Aves, Sphenisciformes): materiales adicionales, status taxonómico y distribución geográfica. *Revista del Museo Argentino de Ciencias Naturales* 6: 233–237.
- ANDO T. 2007. *New Zealand Fossil Penguins: Origin, Pattern, and Process*. Ph.D. Thesis University of Otago, New Zealand: 355 pp.
- BERTELLI S. and GIANNINI N. 2005. A phylogeny of extant penguins (Aves: Sphenisciformes) combining morphology and mitochondrial sequences. *Cladistics* 21: 209–239.
- BERTELLI S., GIANNINI N. and KSEPKA D. 2006. Redescription and Phylogenetic Position of the Early Miocene Penguin *Paraptendytes antarcticus* from Patagonia. *American Museum Novitates* 3525: 1–36.
- CHÁVEZ HOFFMEISTER M. 2007. Propiedades tafonómicas de la ornitofauna del Miembro Bonebed de la Formación Bahía Inglesa (Mioceno Superior), Atacama, Chile. In: J. Calvo, J. Porfiri, B. Gonzalez and D. Dos Santos (eds) *Paleontología y dinosaurios desde América Latina*. Ediunc, Argentina: 79–88.
- CHÁVEZ HOFFMEISTER M., CARRILLO BRICEÑO J. and NIELSEN S. 2014. The Evolution of Seabirds in the Humboldt Current: New Clues from the Pliocene of Central Chile. *PLoS One* 9: e90043.
- CLARKE J., KSEPKA D., SALAS R., ALTAMIRANO A., SHAWKEY M., D'ALBA L., VINTHER J., DEVRIES T. and BABY P. 2010. Fossil evidence for evolution of the shape and color of penguin feathers. *Science* 330: 954–957.
- CLARKE J., KSEPKA D., STUCCHI M., URBINA M., GIANNINI N., BERTELLI S., NARVÁEZ Y. and BOYD C. 2007. Paleogene equatorial penguins challenge the proposed relationship between biogeography, diversity, and Cenozoic climate change. *Proceedings of the National Academy of Sciences of the United States of America* 104: 11545–11550.
- CRUZ I. 2005. La interpretación de partes esqueléticas de aves, patrones naturales e interpretación arqueológica. *Archaeofauna* 14: 69–81.
- CRUZ I. 2007. Avian taphonomy: observations at two magellanic penguin (*Spheniscus magellanicus*) breeding colonies and their implications for the fossil record. *Journal of Archaeological Science* 34: 1252–1261.

- FORDYCE R.E. and JONES C.M. 1990. Penguin history and new fossil material from New Zealand. In: L.S. Davis and J.T. Darby (eds) *Penguin biology*. Academic Press, San Diego: 419–446.
- FORDYCE R.E. and THOMAS D.B. 2011. *Kaiika maxwelli*, a new Early Eocene archaic penguin (Sphenisciformes, Aves) from Waihao Valley, South Canterbury, New Zealand. *New Zealand Journal of Geology and Geophysics* 54: 43–51.
- GIANNINI N. and BERTELLI S. 2004. Phylogeny of extant penguins based on integumentary and breeding characters. *Auk* 121: 422–434.
- GOLOBOFF P., FARRIS J. and NIXON K. 2003. *TNT: Tree Analysis Using New Technology*. Program and documentation, available from the authors, and at www.zmuc.dk/public/phylogeny.
- JADWISZCZAK P. 2006. Eocene penguins of Seymour Island, Antarctica: Taxonomy. *Polish Polar Research* 27: 3–62.
- JADWISZCZAK P. 2011. New data on morphology of late Eocene penguins and implications for their geographic distribution. *Antarctic Science* 23: 605–606.
- JADWISZCZAK P. 2013. Taxonomic diversity of Eocene Antarctic penguins: a changing picture. In: M. Hambrey, P. Barker, P. Barrett, V. Bowman, B. Davies, J. Smellie and M. Tranter (eds) *Antarctic Palaeoenvironments and Earth-Surface Processes*. Geological Society, Special Publications, London, 381: 129–138.
- JADWISZCZAK P. and ACOSTA HOSPITALECHE C. 2013. Distinguishing between two Antarctic species of Eocene *Palaeudyptes* penguins: a statistical approach using tarsometatarsi. *Polish Polar Research* 34: 237–252.
- JADWISZCZAK P. and MÖRS T. 2011. Aspects of diversity in early Antarctic Penguins. *Acta Palaeontologica Polonica* 56: 269–277.
- KSEPKA D. and ANDO T. 2011. Penguins past, present and future: trends in the evolution of the Sphenisciformes. In: G. Dyke and G. Kaiser (eds) *Living Dinosaurs, The Evolutionary History of Modern Birds*. Wiley-Blackwell: 155–186.
- KSEPKA D. and CLARKE J. 2010. The basal penguin (Aves: Sphenisciformes) *Perudyptes devriesi* and a phylogenetic evaluation of the penguin fossil record. *Bulletin of the American Museum of Natural History* 337: 1–77.
- KSEPKA D. and THOMAS D. 2013. Multiple Cenozoic invasions of Africa by penguins (Aves, Sphenisciformes). *Proceedings of the Royal Society B* 279: 1027–1032.
- KSEPKA D., BERTELLI S. and GIANNINI N. 2006. The phylogeny of the living and fossil Sphenisciformes (penguins). *Cladistics* 22: 412–441.
- KSEPKA D., FORDYCE E., ANDO T. and JONES C. 2012. New fossil penguins (Aves: Sphenisciformes) from the Oligocene of New Zealand reveal the skeletal plan of stem penguins. *Journal of Vertebrate Paleontology* 32: 235–254.
- LIVEZEY B. and ZUSI R. 2006. Higher-order phylogeny of modern birds (Theropoda, Aves: Neornithes) based on comparative anatomy: I. methods and characters. *Bulletin of Carnegie Museum of Natural History* 37: 1–544.
- MARPLES J. 1953. Fossil penguins from the mid-Tertiary of Seymour Island. *Falkland Islands Dependencies Survey Scientific Reports* 5: 1–15.
- MARPLES J. 1962. Observations on the history of penguins. In: G. Leeper (ed.) *The evolution of living organisms*. Cambridge University Press, London: 408–416.
- MYRCHA A., JADWISZCZAK P., TAMBUSI C., NORIEGA J., GAŹDZICKI A., TATUR A. and DEL VALLE R. 2002. Taxonomic revision of Eocene Antarctic penguins based on tarsometatarsal morphology. *Polish Polar Research* 23: 5–46.
- O'HARA R. 1989. *Systematics and the study of natural history, with an estimate of the phylogeny of penguins (Aves: Spheniscidae)*. Ph.D. Thesis, Harvard University, Cambridge, 171 pp.
- SIMPSON G.G. 1946. Fossil penguins. *Bulletin of the American Museum of Natural History* 87: 1–99.
- SIMPSON G.G. 1971. Review of fossil penguins from Seymour Island. *Proceedings of the Royal Society of London B* 178: 357–387.

- SLACK K.E., JONES C.M., ANDO T., HARRISON G.L., FORDYCE R.E., ARNASON U. and PENNY D. 2006. Early penguin fossils, plus mitochondrial genomes, calibrate avian evolution. *Molecular Biology and Evolution* 23: 1144–1155.
- SUBRAMANIAN S., BEANS PICÓN G., SWAMINATHAN S., MILLAR C. and LAMBERT D. 2013. Evidence for a recent origin of penguins. *Biology Letters* 9: 20130748.
- WALSH S., MCLEOD N. and O'NEIL M. 2007. Spot the penguin: Can reliable taxonomic identifications be made using isolated foot bones. In: N. McLeod (ed.) *Automated Taxon Identification in Systematics: Theory, Approaches and Applications*. CRC Press, Boca Raton: 225–238.
- WALSH S., MCLEOD N. and O'NEIL M. 2008. Analysis of spheniscid humerus and tarsometatarsus morphological variability using DAISY automated image recognition. *Oryctos* 7: 129–136.

Received 30 July 2014

Accepted 9 September 2014

Appendix 1

The corrected dataset comprising humerus and tarsometatarsus characters. Multi-state characters are coded as follows: [01] = A, [12] = B, [23] = C, [02] = D, [012] = E. For more details, see Character descriptions.

Gavia immer

010----0200--10-0000000000-000-2-03011--000100011000101010A1000010000020001

Diomedea exulans

000----0200--00-0000000000-000-3-03000--00110000100021001001000000021000201

Oceanodroma tethys

000----0200--10-0010000000-000-2-03011--00100010230001101010000000010110001

Puffinus griseus

000----0200--10-0000000000-000-3-03010--00110020230011001001000000010000201

Pelecanoides urinatrix

000----0200--10-0021000000-000-2-03010--00110120230011001001000000010000201

Aptenodytes patagonicus

12210012122002112222213011003110012223023120100002002200111A0000212C2110001

Pygoscelis papua

12220A12222002112222213011003110A122231230B01A100200221A1A10000A2B2CD010000

Megadyptes antipodes

12220112222002112222213011003A1011122312212010000200220011A100002B2B0110010

Eudyptes chrysocome

1222A11BB22002112222213011003A10A1222312C010101002002C0D11010001222C2110010

Eudyptula minor

12210112222002112221113011002010A1B223A2B02010100D00B20211A100022323D1101?1

Spheniscus humboldti

1221A11222211210122BB13011003110BB1223A2C11A1A2002002C021B010002232C01101A0

Madrynornis mirandus

122200111220021122222130110020100111230220101010020023021101100221231110000

Palaeodyptes klekowskii

121000000210?2011221012A00102100?2002300301000000?0122012100000020232001001

Palaeodyptes gunnari

1210A000021002011221012A0010BA0012002300201000100?0?22??21A0000A2023B001001

Anthropornis nordenskjoldi

121000?00210?2011221013A001130?0?20023001????0?0?0??2?0010??10212????????

Anthropornis grandis

12101010021??201?221?120001130?0?00??0201010?00????2?00010001021????01??0

Notodyptes wimani

??30?01?100?0???01110000020????01???

Delphinornis arctowskii

??201010100201220110100002201?0100100

Delphinornis gracilis

??101010100?01?30?1110100?20??000?111

Delphinornis larseni

??201010A0010113011010A00220122000101

Mesetaornis polaris

??101010100?0????110101002201?010?101

Marambiornis exilis

??10101010010113011010100220??0100101

Perudyptes devriesi

121000100010?2011111002000011111??202300?????????????????????????????????0?20232110000

Kaiika maxwelli

12100010001002001111?0100?0110?1??10??

Crossvallia unienwillia

121010?0001??20??111??00?011011-?10220??

Waimanu tuatahi

121010100010?2001111?0?000010011-02022000??0??00?0??0?1001?1??200210000?1